

## Cellular-automata calculation of frequency-dependent permeability of porous media

Mark A. Knackstedt

*Department of Mathematics, University of Melbourne, Parkville, Victoria 3052, Australia  
and Department of Applied Mathematics, Research School of Physical Sciences and Engineering, The Australian National University,  
G.P.O. Box 4, Canberra, Australian Capital Territory 2601, Australia\**

Muhammad Sahimi

*Department of Mathematics, University of Melbourne, Parkville, Victoria 3052, Australia;  
Department of Chemical Engineering, University of Southern California, Los Angeles, California 90089;\*  
and HLRZ Supercomputer Center, c/o Kernforschungsanlage Jülich G.m.b.H., Postfach 1913, W-5170 Jülich 1, Germany*

Derek Y. C. Chan

*Department of Mathematics, University of Melbourne, Parkville, Victoria 3052, Australia  
(Received 3 September 1992)*

We use a cellular-automata (CA) method to determine the frequency-dependent permeability  $k(\omega)$  of a channel and a disordered porous medium. The CA results for the channel flow agree completely with the analytical solution of the problem. For flow in a porous medium, we calculate  $k(\omega)$  over a wide range of the frequencies  $\omega$  and for several values of the porosity. Our CA results for disordered porous media support the relation  $k(\omega)/k_0 = f(\omega/\omega_c)$ , where  $k_0$  is the static permeability of the medium,  $\omega_c$  is a characteristic frequency, and  $f(x)$  is a *universal* function, proposed previously, based on experimental data.

PACS number(s): 47.55.Mh, 47.15.Gf

### I. INTRODUCTION

Flow phenomena in porous media are important to a wide variety of problems and have been studied for a long time [1]. Problems as diverse as enhanced recovery of oil from underground reservoirs, drainage and imbibition in soil, mercury porosimetry in a porous catalyst for determining its pore-size distribution, and many other processes are all in this class of phenomena.

One of the most important properties of a porous medium is its effective permeability, which is a measure of its ability for allowing fluid flow to take place. For this reason, calculating the effective permeability and relating it to the microstructure of the porous medium has been a problem of great interest for many decades. Since the effective permeability depends on the microstructure of the medium, many models of pore space have been developed, and many numerical and analytical techniques have also been suggested for determining their permeabilities. However, most of such models are very simple; otherwise computations become almost impossible. But this is now changing rapidly, as new computer simulation techniques [2] are allowing us to develop highly efficient algorithms for determining the effective permeability and other transport properties of porous media. Among these are cellular-automata (CA) methods [3–5] which, in the context of fluid flow problems, are the discrete solutions of the Navier-Stokes equations. In the past few years, CA methods have been used by many authors [6–14] for investigating various flow phenomena in porous media.

Most of the previous studies of flow phenomena using

CA methods were restricted to the steady-state condition. Time was involved only during the relaxation process for reaching the steady-state condition. One notable exception is the work of Lim [15], who studied boundary layer flows. Lim's work indicates that the CA methods can be used for studying dynamical flow problems. In a previous paper [16], we reported preliminary results for *dynamic* (frequency-dependent) permeability of a porous medium, defined by

$$\mathbf{V}(\omega) = -\frac{k(\omega)}{\mu} \nabla P(\omega), \quad (1)$$

where  $\mathbf{V}$  is the average fluid velocity,  $k(\omega)$  is the permeability at frequency  $\omega$ ,  $\mu$  is the viscosity of the fluid, and  $P$  is the pressure. Dynamics is introduced into the system by setting  $P = Pe^{-i\omega t}$  as the ac pressure between two opposite faces of a porous medium at time  $t$ . Equivalently, an oscillatory inlet flow velocity can be imposed on the system. There are already some experimental data for  $k(\omega)$  [17] measured in fused-glass beads. Very simple models of porous media have also been used to investigate the problem theoretically [18–20]. Instead of studying the response of the porous medium to an oscillatory pressure gradient, our previous paper [16] only looked at the response of the system to a unit step input. This was necessitated by the computational difficulties at that time and, in fact,  $k(\omega)$  was not calculated. In the present paper, we present the results of a full investigation of the problem in both a channel and a porous medium. The advantage of CA methods is that they allow us to calculate  $k(\omega)$  for complex and realistic models of porous media, a task that is very difficult with any other method.

In Sec. II, we give the details of the model and the simulations, and then, present the results for channel and porous-media flows.

## II. CA METHODS FOR DYNAMIC PERMEABILITY

We studied dynamic permeability of both a channel and a two-dimensional model porous medium. The motivation for studying the problem in a channel is that one can derive the analytical solution of the problem and, thus, compare it with the CA results to assess their accuracy. The simulations were carried out with a system of size  $L_x \times L_y$ , with  $L_x = 2048$  and  $L_y = 512$ , where  $L_x$  and  $L_y$  are the length and width of the channel, respectively. To generate the porous medium, we placed at random hexagonal obstacles in the channel to reach a desired porosity, i.e., the volume fraction of the pores between the obstacles. To eliminate the end effects, we only packed the central  $\frac{3}{4}$  of the channel with the hexagons, and even then performed all of our measurements in the central half of the system. The porosity was also calculated based on the central half of the system. As discussed by Kohring [11], if the size of the obstacles is not large (much larger than the mean-free path of the particles), then true hydrodynamic regime may not be obtained, and the results may be dependent on the obstacles' size. Thus, we used large hexagons (the size of their sides was 20 lattice bonds) to avoid this difficulty. Reflecting boundary conditions on the surface of the obstacles and on the channel's walls were used to mimic the usual no-slip boundary condition at a solid surface. Particle density in the simulations was one particle per site. Simulations start by distributing the particle velocities in the system in such a way that the fluid is macroscopically at rest. Note, however, that in agreement with the range of validity of Darcy's law (i.e., very low Reynolds number), and in order to simulate incompressible flows, the average flow velocities have to be low enough. We then iterated the system 5000 time steps to allow it to relax, where each time step corresponds to updating the state of all of its nodes according to the usual rules of two-dimensional CA. A time-dependent velocity wave was then introduced at the inlet of the system, and the system's response was monitored. The velocity wave was either Gaussian with given mean and standard deviations, or sinusoidal with a given period. The maximum flow velocity introduced at the inlet was chosen in all cases to be 0.2 (lattice bond/time step), which is small enough for the nonlinearities, which arise at higher velocities, to be negligible. To introduce the wave into the system, we simply biased the motion of the particles at the entrance, i.e., change the particles' velocities at the inlet so that the flow velocity there matches the velocity wave. The effect of the velocity wave has to be relatively strong for its effect to be measured downstream. Typically, the period of time during which we introduced the velocity wave into the system was 200–1000 time steps, after which the wave was withdrawn. In the next 20 000 time steps, the average flow velocity and pressure gradient of the system were measured, although in all cases the effect of the velocity wave died out after about 7000 time steps.

Up to 180 different realizations of the system were used, and the average values were calculated. We then used a standard discrete Fourier transform [21] to convert the measured  $V_x(t)$  and  $\nabla P(t)$  into frequency-dependent quantities, and used Eq. (1) to calculate  $k(\omega)$ . In our previous paper [16], a unit step velocity was used to disturb the system. However, the measurements there proved to be too noisy to yield any reliable results, which was the chief reason we did not calculate  $k(\omega)$ .

## III. DYNAMIC PERMEABILITY OF A CHANNEL

In this section, we compare the CA results with the analytical solution of the problem in a channel. Let  $y$  denote the transverse coordinate (i.e., perpendicular to the macroscopic flow), and  $a$  be the width of the channel. If we let  $V_x = -i\omega W$ , where  $V_x$  is the macroscopic velocity in the axial direction, then the Navier-Stokes equations, in the Fourier space, are simplified to

$$\frac{d^2 W}{dy^2} + i\omega W = -\frac{i}{\omega}, \quad (2)$$

subject to no-slip boundary conditions on the channels walls, i.e., at  $y=0$  and  $y=a$ . The solution of Eq. (2) is given by

$$W(y) = \frac{1}{\omega^2} \left[ \frac{1 - \cos(\beta a)}{\sin(\beta a)} \sin(\beta y) + \cos(\beta y) - 1 \right], \quad (3)$$

where  $\beta = (i\omega)^{1/2}$ . From Eq. (3), the frequency-dependent permeability is given by

$$k(\omega) = -\frac{i\omega}{a} \int_0^a W(y) dy = \frac{i}{\omega} \left[ 1 - \frac{2}{\beta a} \frac{1 - \cos \beta a}{\sin \beta a} \right]. \quad (4)$$

Since  $(i\omega)^{1/2} = (2\omega)^{1/2}(1+i)/2$ , if we write  $k(\omega) = k_r + ik_i$ , we can easily obtain the real and imaginary part of  $k(\omega)$ . It is straightforward to show that, as  $\omega \rightarrow 0$ ,

$$k(\omega) \rightarrow \frac{a^2}{12} - i \frac{a^4 \omega}{72}, \quad (5)$$

so that in the limit  $\omega=0$ , i.e., very long times, we recover the usual relation,  $k(0) = k_0 = a^2/12$ , for the static permeability of the channel. Note that for a tube of radius  $a$ , the corresponding dynamic permeability is given by [20]

$$k(\omega) = \frac{i}{\omega} \left[ 1 - \frac{2}{\beta a} \frac{J_1(\beta a)}{J_0(\beta a)} \right], \quad (6)$$

where  $J_i$  is the Bessel function of order  $i$ .

Figures 1 and 2 show typical time variations of the velocity and pressure gradient measured downstream in the channel flow. The pressure gradient is calculated as follows. We first measure the pressure along the channel, and then find the best (least-squares) fit to the measurements. This explains why the pressure gradient is noisy, whereas the velocity is relatively noise free. After the system is perturbed by the wave at the inlet, they both change sharply, but as the effect of the perturbation dies out, they both reduce to zero again. It is this noise at both ends of the pressure gradient that makes calculating its Fourier transform difficult. In fact, this noise persists

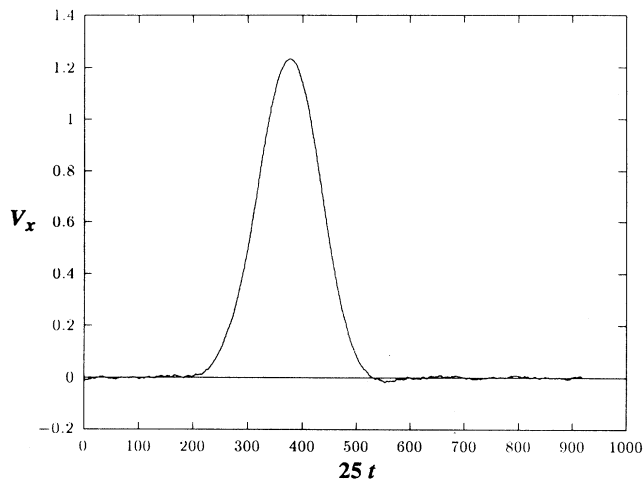


FIG. 1. Time variations of the fluid velocity in the channel obtained with CA.

even with a very large system and, therefore, it is necessary to make many different realizations (different initial distributions of the particles and their velocities) of the system, calculate the average velocity and pressure-gradient profiles, and Fourier transform the *average values*. The range of the frequencies that can be measured by the CA method is bounded on the low-frequency end by the length of the time over which the measurements are done, and at high frequencies by the noise in the pressure gradient.

Figure 3 compares the CA results for the dynamic permeability of the channel with the analytical solution, and the agreement is excellent. For large values of  $\omega$  (i.e., very short times), we have

$$k(\omega) = a_1 \omega^{-3/2} + i a_2 \omega^{-1}, \quad (7)$$

where  $a_1$  and  $a_2$  are constant. Our CA results agree with

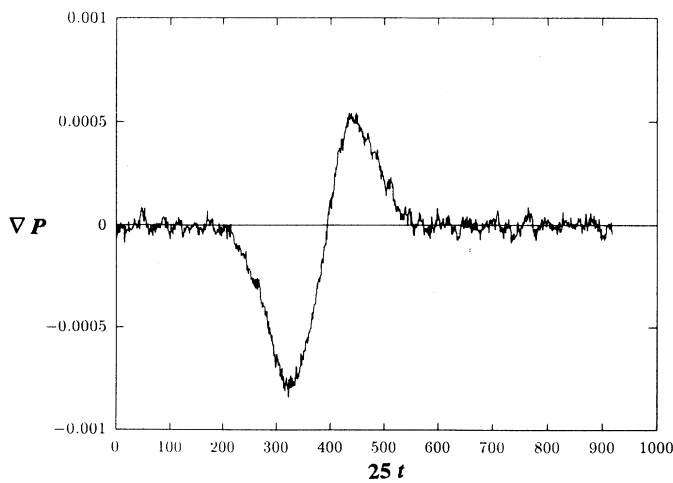


FIG. 2. Time variations of the pressure gradient in the channel obtained with CA.

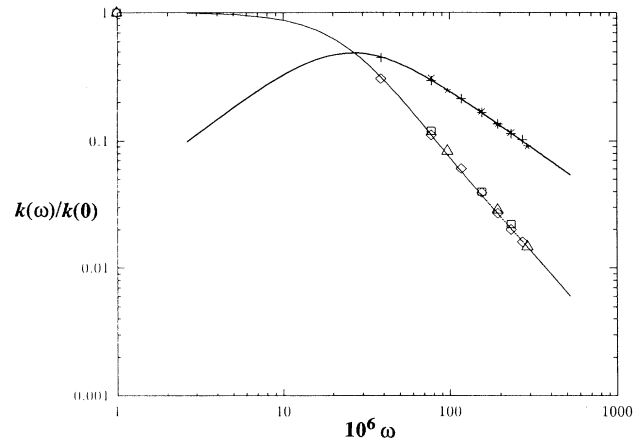


FIG. 3. Frequency dependence of the channel permeability  $k(\omega)$ , where  $+$  denotes the real part of  $k(\omega)$ , and the other symbols show its imaginary part obtained with different inlet velocity waves. Solid curves are the analytical solution of the problem.

Eq. (7). Equation (7) also tells us that if we were to use a random resistor network model of porous media for calculating  $k(\omega)$  at large values of frequencies, the bonds of the network would not be linear elements, but would have a nonlinear and unusual frequency dependence. The agreement between the CA results and the analytical solution for the channel flow confirms the validity of the CA method for calculating  $k(\omega)$ . We thus turn to flow in a model porous medium.

#### IV. FREQUENCY-DEPENDENT PERMEABILITY OF POROUS MEDIA

We first ensured that the results for porous media are insensitive to the form of the velocity wave with which the system was perturbed. Figure 4 presents the frequen-

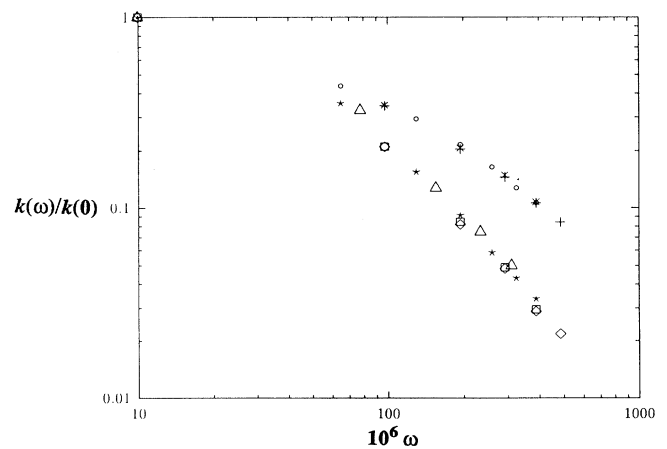


FIG. 4. Frequency dependence of the dynamic permeability of the porous medium at  $\phi=0.94$ , obtained with three different velocity waves. The upper symbols show the imaginary part, while the lower ones show the real part.

cy dependence of  $k_r$  and  $k_i$  at a porosity  $\phi=0.94$ , for three different waves. Two of these are Gaussian with a standard deviation of 200 and 500, while the third one is a sinusoidal wave with a period of 300. As can be seen, there is no difference between the permeabilities of the three systems. For large  $\omega$ , the behavior of  $k(\omega)$  is obtained by a least-square fit of the results. For the results shown in Fig. 4, we obtained  $k_r(\omega)\sim\omega^{-1.47}$  and  $k_i(\omega)\sim\omega^{-1.0}$ , both of which agree with Eq. (7). Figure 5 shows the result for  $\phi=0.87$ . In this case, we found  $k_r(\omega)\sim\omega^{-1.46}$  and  $k_i(\omega)\sim\omega^{-0.97}$ , again in agreement with Eq. (7).

The real and imaginary parts of the velocity profile represent, respectively, the viscous and inertial effects. For small values of  $\omega$  (long times), the real part is much larger than the imaginary part. However, with increasing  $\omega$  the imaginary part also increases, and at some characteristic frequency  $\omega_c$ , it becomes larger than the real part. Thus,  $\omega_c$  signals the point at which the inertial effects become larger than the viscous effects. The value of  $\omega_c$  is approximately the frequency at which  $k_i$  achieves its maximum (see Fig. 3). In Fig. 6, we show the results for  $\phi=0.79$ , and as can be seen, there is a large shift in  $\omega_c$  (i.e., the curves essentially start at the maximum), as a result of which one can no longer discern the high-frequency behavior of  $k(\omega)$ . As the porosity of the medium decreases,  $\omega_c$  increases rapidly. Johnson, Koplik, and Dashen [18] proposed that

$$\omega_c = \frac{\mu}{Fk_0\rho} = \frac{\mu\phi}{\rho k_0 T}, \quad (8)$$

where  $\rho$  is the fluid density and  $T$  is the tortuosity of the medium. Here  $F=\sigma_f/\sigma$  is the formation factor of the porous medium, where  $\sigma$  is the effective electrical conductivity of the porous medium saturated with a fluid with electrical conductivity  $\sigma_f$ . With decreasing  $\phi$ ,  $F$  increases, but the decrease in  $k_0$  is much faster than the increase in  $F$  and, therefore,  $\omega_c$  also increases. This means

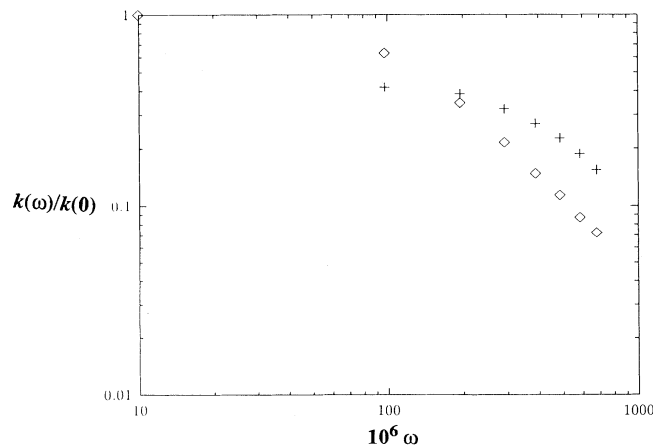


FIG. 5. Frequency dependence of the real part  $k_r$  (diamonds) and imaginary part  $k_i$  (+) of the permeability at porosity  $\phi=0.87$ .

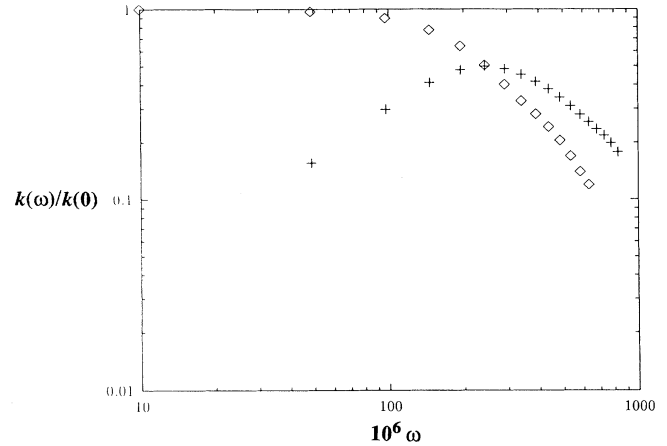


FIG. 6. Frequency dependence of  $k_r$  and  $k_i$  for  $\phi=0.79$ . Symbols are the same as in Fig. 5.

that with decreasing  $\phi$ , the characteristic frequency  $\omega_c$  shifts to very large values, which then implies that in order to locate  $\omega_c$  we have to do all of the measurements at very short times. However, at such short times the noise generated by the CA pressure or velocity is too high, which makes it difficult to do any meaningful measurements. Nevertheless, we can obtain the low-frequency behavior of  $k(\omega)$  at this porosity. This difficulty is *not* a feature of CA methods, but is shared by all methods and models of calculating  $k(\omega)$ . Our results indicate that for small  $\omega$ ,  $k_i\sim\omega$ , while  $k_r$  is essentially constant, both of which are in agreement with Eq. (5). The conclusion is that Eqs. (5) and (7) continue to hold for porous media, at least for the range of porosities that we studied, but with decreasing  $\phi$  it becomes increasingly more difficult to obtain the high-frequency behavior of  $k(\omega)$ . We expect Eqs. (5) and (7) to hold for any nonfractal porous medium.

It has been suggested [17–20] that, regardless of the value of  $\phi$ , the dynamic permeability obeys a simple scaling law

$$\frac{k(\omega)}{k_0} = f(\omega/\omega_c), \quad (9)$$

where  $f$  is a universal function *independent* of the microstructure of the medium. The universality of  $f$  is, of course, a disappointing result, because it indicates that measurements of  $k(\omega)$  do *not* provide any information about the microstructure of the porous medium. However, Johnson, Koplik, and Dashen [18] showed that the high-frequency values of  $k(\omega)$  can provide information about a parameter that might provide a link between  $k_0$  and  $\sigma$ , an outstanding unsolved problem. Using our CA results, we checked whether Eq. (9) is obeyed. Figure 7 shows the collapse of our results for  $\phi=1, 0.94, 0.89$ , and  $0.79$ , and it is clear that the collapse is complete and, therefore, Eq. (9) is obeyed. This is a confirmation of Eq. (9) for a realistic and complex model of a porous medium. Johnson [22] has shown that a large number of equations with certain appropriate properties obey Eq. (9), and

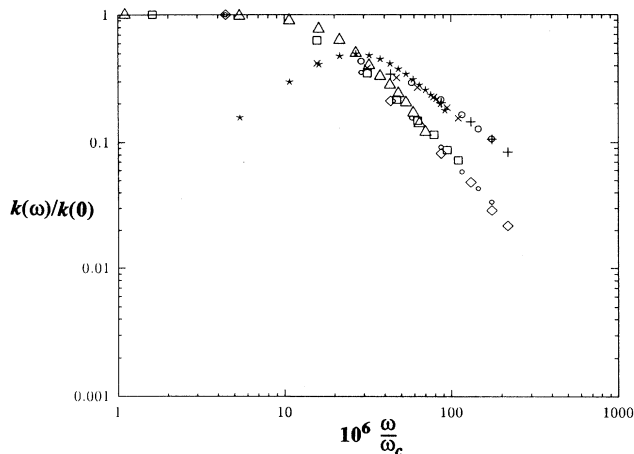


FIG. 7. Scaling of  $k(\omega)/k_0$  with  $\omega/\omega_c$ . The curve with a maximum shows the imaginary part.

Johnson, Koplik, and Dashen [18] gave one simple example of such functions.

### V. SUMMARY

We calculated frequency-dependent permeabilities of a channel and a model porous medium using a cellular-automata method. The results for the channel flow were in complete agreement with the analytical solution of the

problem. The results for porous media indicated that the frequency dependence of the dynamic permeability found for the channel flow continue to hold for the porous-media flow. Moreover, the ratio of the dynamic and static permeabilities follows a universal scaling function of  $\omega/\omega_c$ , where  $\omega_c$  is a characteristic frequency at which the inertial effects exceed the viscous effects, which is in agreement with experimental data.

### ACKNOWLEDGMENTS

We would like to thank Greg Kohring for allowing us to use his highly efficient CA program, Dietrich Stauffer for encouragement and a critical reading of the manuscript, and the Parallel Computing Research Facility of the Australian National University for generous allocation of computer time on their CM2 computer. Part of this work was carried out while two of us (M.A.K. and M.S.) were visiting the Department of Mathematics of the University of Melbourne, Australia. They would like to thank Barry Hughes and Lee White for warm hospitality. M.S. would also like to thank the Advanced Mineral Products Centre and the Department of Mathematics of the University of Melbourne for financial support. This paper was prepared while M.A.K. and M.S. were visiting the HLRZ Supercomputer Center at KFA Jülich, Germany. They would like to thank the Center and Hans Herrmann for warm hospitality. M.S. is grateful to the Alexander von Humboldt Foundation, and Grant BMFT No. 0326657D for financial support.

\*Present and permanent address.

- [1] M. Sahimi, *Rev. Mod. Phys.* (to be published).
- [2] K. Binder, *Applications of Monte Carlo Methods* (Springer, Berlin, 1987).
- [3] U. Frisch, B. Hasslacher, and Y. Pomeau, *Phys. Rev. Lett.* **56**, 1505 (1986).
- [4] D. H. Rothman, *Geophysics* **53**, 509 (1988).
- [5] Special issue on NATO ARW on Lattice Gas Methods for PDE's, *Physica D* **47** (1) (1991).
- [6] S. Chen, G. D. Doolen, and W. H. Mathaues, *J. Stat. Phys.* **64**, 1133 (1991).
- [7] D. H. Rothman and J. M. Keller, *J. Stat. Phys.* **52**, 1119 (1988).
- [8] U. Brosa and D. Stauffer, *J. Stat. Phys.* **63**, 405 (1991).
- [9] A. Cancelliere, C. Chang, E. Foti, D. H. Rothman, and S. Succi, *Phys. Fluids A* **2**, 2085 (1990).
- [10] M. Sahimi and D. Stauffer, *Chem. Eng. Sci.* **46**, 2225 (1991).
- [11] G. A. Kohring, *J. Phys. II France* **1**, 593 (1991).
- [12] G. A. Kohring, *Int. J. Mod. Phys. C* **2**, 755 (1991).
- [13] G. A. Kohring, *J. Phys. II France* **2**, 265 (1992).
- [14] J. A. M. S. Duarte and U. Brosa, *J. Stat. Phys.* **60**, 501 (1990).
- [15] H. A. Lim, *Phys. Rev. A* **40**, 968 (1989).
- [16] J. A. M. S. Duarte, M. Sahimi, and J. M. de Carvalho, *J. Phys. II France* **2**, 1 (1992).
- [17] E. Charlaix, A. P. Kushnik, and J. P. Stokes, *Phys. Rev. Lett.* **61**, 1595 (1988).
- [18] D. L. Johnson, J. Koplik, and R. Dashen, *J. Fluid Mech.* **176**, 379 (1987).
- [19] P. Sheng and M.-Y. Zhou, *Phys. Rev. Lett.* **61**, 1591 (1988).
- [20] M.-Y. Zhou and P. Sheng, *Phys. Rev. B* **39**, 12027 (1989).
- [21] W. H. Press, B. P. Flannery, S. A. Teukolsky, and W. T. Vetterling, *Numerical Recipes* (Cambridge University Press, Cambridge, 1985).
- [22] D. L. Johnson, *Phys. Rev. Lett.* **63**, 580 (1989).